Applied Catalysis B: Environmental 150–151 (2014) 402–410

Contents lists available at ScienceDirect

Applied Catalysis B: Environmental

journal homepage: www.elsevier.com/locate/apcatb

Wet Air Oxidation of phenol over Pt and Ru catalysts supported on cerium-based oxides: Resistance to fouling and kinetic modelling

Sylvain Keav[a,b,*], Alejandra Espinosa de los Monteros[b], Jacques Barbier Jr.[b], Daniel Duprez[b]

[a] Empa, Swiss Federal Laboratories for Materials Science and Technology, Laboratory for Solid State Chemistry and Catalysis, Ueberlandstrasse 129, CH-8600 Dübendorf, Switzerland
[b] IC2MP, UMR 7285, University of Poitiers and CNRS, 4 rue Michel Brunet, 86022 Poitiers Cedex, France

ARTICLE INFO

Article history:
Received 1 October 2013
Received in revised form
13 December 2013
Accepted 16 December 2013
Available online 24 December 2013

Keywords:
CWAO
Phenol
Noble metal
OSC
Deactivation

ABSTRACT

Ceria and doped ceria supported Pt and Ru catalysts were tested at 160 °C in the Catalytic Wet Air Oxidation (CWAO) of phenol. Catalysts were compared in terms of activity, selectivity and resistance towards fouling. The respective influences of metal phase and support were studied. Under the selected operating conditions, 100% phenol conversion could be reached. Contrary to what was expected, improved Oxygen Storage Capacities (OSC) accelerated the accumulation of adsorbed species on the catalyst surface, therefore limiting the catalytic performance. By contrast, high metal dispersions enhanced both the elimination of aqueous organic compounds and the degradation of heavy molecules involved in the catalyst fouling. The progressive decrease in activity induced by carbonaceous deposits could be kinetically modelled using a simple reaction scheme.

1. Introduction

Known since the early 20th century, the Wet Air Oxidation (WAO) process is particularly promising for the treatment of wastewaters containing highly concentrated, toxic or hardly biodegradable compounds [1]. WAO consists in oxidizing organic pollutants into nontoxic products (ultimately CO_2 and H_2O). In the absence of a catalyst, temperatures up to 320 °C and pressures up to 200 bar are necessary to attain acceptable conversions. The use of a catalyst significantly improves the efficiency of the process: Catalytic Wet Air Oxidation (CWAO) can be operated at temperatures and pressures below 200 °C and 30 bar, respectively.

Many heterogeneous catalytic systems have been considered for the reaction. Amongst them, supported Pt, Ru and Pd noble metals demonstrate high stability and activity. Due to their efficiency in processes involving redox reactions as well as their stability under acidic and oxidative conditions, cerium-based oxides are excellent candidates as supports for WAO catalysts. It was shown that ceria alone is able to convert more than 90% of aqueous phenol [2] and that its addition to certain formulations can greatly improve the catalytic performance [3]. Additionally, some cerium-based oxides, such as MnO_2–CeO_2, are extremely active in the oxidation of refractory compounds [4]. The efficiency of such catalytic systems comes from the oxygen transfer and storage properties of ceria, which result from the ability of Ce element to easily switch between +III and +IV oxidation states. The mobility of oxygen atoms can be improved by heat treatment, doping or the presence of noble metal species dispersed on the oxide surface [2,5].

Phenol is an intermediate in the oxidation of many aromatic compounds. Moreover, it is a toxic molecule resistant to biotreatment. Several authors determined the reaction pathway of the catalytic oxidation of aqueous phenol [6–8]. One of the most elaborated models, proposed by Rivas et al. [9], was based on elementary radical reactions (phenol oxidation is recognized to proceed via a free-radical mechanism [10]). The authors calculated unknown rate constants and verified that predicted concentration profiles were in agreement with experimental data. Eftaxias et al. [11] carried out a noteworthy kinetic study of phenol oxidation: a scheme comprising 7 reactions was considered and 31 parameters were simultaneously optimized. However, these reaction pathways do not take into account the formation of deactivating polymeric species. A few counterexamples can be found. Alejandre et al. [12] considered the direct polymerization of phenol. Masende et al. [13] proposed a particularly interesting scheme in which they specified desired and

* Corresponding author at: Empa, Swiss Federal Laboratories for Materials Science and Technology, Laboratory for Solid State Chemistry and Catalysis, Ueberlandstrasse 129, CH-8600 Dübendorf, Switzerland. Tel.: +41 587 654 726.
E-mail address: sylvain.keav@empa.ch (S. Keav).

0926-3373/$ – see front matter © 2013 Elsevier B.V. All rights reserved.
http://dx.doi.org/10.1016/j.apcatb.2013.12.028

undesired reaction routes. Pintar and Levec [10] included the formation of heavy species from polymerization reactions involving glyoxal. More recently, Delgado et al. [14] included the formation and oxidation of the carbonaceous deposits as a parallel pathway for phenol degradation. Hamoudi et al. [15] as well as Arena et al. [16,17] proposed lumped reaction schemes taking account of adsorption and desorption steps of reactants and products as well as activity decline due to the formation and accumulation of carbonaceous materials over the catalytic surface.

This paper deals with CWAO of phenol in the presence of Pt and Ru catalysts supported on Ce-, Zr- and Pr-based oxides. It focuses on the respective influences of metal and support phases on activity and selectivity. Deactivation by fouling is considered and modelled via a simple reaction scheme.

2. Experimental

2.1. Catalyst preparation

CeO_2 (Ce), $Zr_{0.1}Ce_{0.9}O_2$ (ZrCe) and $Zr_{0.1}(Ce_{0.75}Pr_{0.25})_{0.9}O_2$ (ZrCePr) were used as supports in this study. Ce was a commercial HSA5 ceria provided by Rhodia and calcined in air at 650 or 800 °C. ZrCe and ZrCePr mixed oxides were synthesized following the sol–gel procedure described by Rossignol et al. [18]: an aqueous solution of $Ce(NO_3)_3{\cdot}6H_2O$ and/or $Pr(NO_3)_3{\cdot}6H_2O$ was progressively added, at room temperature, to a solution of $Zr(OC_3H_7)_4$ in isopropanol. The resulting pseudo-gel was dried in a sand bath at 60 °C for 60 min and subsequently in a ventilated oven at 120 °C for 720 min. The powder was finally calcined in air at 400, 500, 650 or 800 °C for 300 min.

The metal phase was deposited by contacting the bare support with a precursor solution under pH conditions favouring the dispersion of metal species. Catalysts were prepared from $RuCl_3{\cdot}nH_2O$ in acidic medium or $Pt(NH_3)_4(OH)_2$ in alkaline medium. Metal contents were set at 1.25 wt% for Ru and 2.50 wt% for Pt. These values correspond to similar molar amounts of metal species. The mixture of precursor solution and support was stirred at 45 rpm for 240 min and evaporated under vacuum at 30 °C. Final catalysts were obtained after overnight drying at 120 °C followed by reduction in H_2 (30 mL min^{-1}) at 350 or 500 °C for 180 min.

Catalysts with different compositions and calcination/reduction temperatures were synthesized in order to evaluate the influence of the support, the metal phase and the particle size on activity and selectivity. The following notation system was used to name activated catalysts: MeSuppT_{Calc}-T_{Red} where (i) Me is the deposited metal (Ru or Pt), (ii) Supp is the support (Ce, ZrCe or ZrCePr), (iii) T_{Calc} (°C) is the calcination temperature of the support and (iv) T_{Red} (°C) is the reduction temperature of the final catalyst.

2.2. Experimental set-up and procedure

Fouling is the major cause of deactivation of noble metal catalysts used in the CWAO of phenol [19,20]. Since this study focuses on deactivation, operating conditions accelerating the formation of fouling materials (low temperature, high phenol concentration) were selected. CWAO tests were performed in a 0.44 L batch reactor made of Hastelloy C22 alloy loaded with V_{Liq} = 0.16 L of an aqueous solution containing phenol and the catalyst at respective concentrations of C_{PhOH} = 2.098 g L^{-1} and C_{Cat} = 4 g L^{-1}. After a purge with helium, the reactor was heated up to the reaction temperature, typically T = 160 °C. The stirring speed was set at ω = 1000 rpm. At the initial time of the reaction, 20 bars of pure O_2 were introduced into the reactor. The pressure was maintained constant throughout the experiment by regularly refilling with O_2. Gas phase and liquid phase samples were simultaneously and periodically collected for analysis. After 180 min of reaction, the reactor was cooled down to room temperature. The catalyst was recovered, washed with ultra-pure water and dried overnight at 120 °C.

As the reactor was not equipped with a cooling system and since phenol oxidation is an exothermic reaction, a slight increase in temperature (always smaller than 8 °C) was generally recorded, just after introduction of oxygen in the system. Temperature was always back to 160 °C within 2 min. This brief shift from the intended reaction temperature is not expected to significantly affect kinetic data. It is to be noted that, although maintaining constant the operating pressure by refilling oxygen, CO_2 is accumulating in the gas phase during the reaction (CO_2 partial pressure was about 1.5 bar at the end of the experiment with our best performing catalyst). The reproducibility of the experimental protocol was verified for several reference catalysts and the experimental error was found to be lower than 5%. The stirring speed and the mass of catalyst were varied according to well-known procedures [21] in order to confirm the absence of external mass transfer limitations under the selected conditions.

2.3. Analytical techniques

The amount of CO_2 in the gas phase was determined by gas chromatography (Varian 3900 GC equipped with a thermal conductivity detector and a Porapaq Q column). Calculations were made based on the peak surface areas of CO_2 and O_2 in the gas chromatogram as well as the temperature and the total pressure in the CWAO reactor. CO_2 in the liquid phase was quantified from the amount of gaseous CO_2 according to a previous study concerning aqueous/gaseous CO_2 equilibrium at different temperatures and at acidic pH [22]. Phenol and acetic acid in liquid samples were quantified by HPLC using an Aminex HPX87H Biorad column and an UV6000LP diode array detector. Total Organic Carbon (TOC) was measured on a Total Organic Carbon Analyzer 1020A from O.I. Analytical using the TC-IC method.

X-ray diffraction (XRD) patterns were obtained on a θ-θ Bruker D5005 diffractometer using Cu(Kα) radiation (λ = 1.54186 Å) on the 20–60° 2θ interval ($\Delta 2\theta$ = 0.06°; 2 s/step). BET specific surface areas (SSA) were determined via nitrogen adsorption at −196 °C on a Micromeritics Tristar 3000 apparatus after degassing at 250 °C for 120 min under vacuum. Support particle size (d) was calculated from XRD patterns using the Scherrer equation (Eq. (1)) where K = 0.9 is the Scherrer constant, λ (m) is the X-ray wavelength and β (rad) is the full width at half maximum corrected for instrumental broadening) and from SSA assuming quasi-crystalline spherical particles (Eq. (2) where ρ (g m^{-3}) is the density of the oxide).

$$d_{XRD}(\mathrm{m}) = \frac{K \cdot \lambda}{\beta \cdot \cos\ \theta} \quad (1)$$

$$d_{SSA}(\mathrm{m}) = \frac{6 \cdot \rho}{SSA} \quad (2)$$

Oxygen Storage Capacity (OSC) values were measured at atmospheric pressure and 400 °C in a U-shaped reactor continuously purged with He. The sample (5 mg) was first saturated with oxygen and then purged for 10 min. OSC values were determined from the amount of CO_2 formed consecutively to CO injections under CO/O_2 alternate pulse conditions. In the case of supported metal catalysts, measured OSC values were corrected (Eq. (3)) to take account of the formation of surface PtO and bulk RuO_2 and their participation to CO consumption. The number of layers of oxygen atoms involved in the oxygen storage process (NL) was calculated from Eq. (4), where OSC_{Surf} is the theoretical number of reducible surface

Table 1
Specific surface area (SSA), support particle size (d_{SSA}, d_{XRD}), metal dispersion (D), Oxygen Storage Capacity (OSC) and number of layers of available oxygen atoms (NL) of prepared supports and catalysts.

Sample	SSA ($m^2\,g^{-1}$)	d_{SSA} (nm)	d_{XRD} (nm)	D (%)	OSC ($\mu mol_O\,g^{-1}$)	NL
Ce650	97	9	8	–	97	0.18
ZrCe650	73	12	9	–	164	0.44
ZrCePr650	43	20	12	–	346	1.58
RuCe800_350	44	19	16	3.0	353	1.41
RuZrCe500_350	72	12	9	23.0	679	1.83
RuZrCePr650_350	43	20	12	7.0	512	2.33
RuZrCePr800_350	21	40	17	9.1	705	6.58
RuZrCePr800_500	25	34	17	5.0	597	4.68
PtCe800_350	48	17	15	42.0	107	0.39
PtZrCe400_350	59	14	11	52.0	492	1.62
PtZrCePr800_350	22	38	15	21.0	565	5.04
PtZrCePr800_800	12	70	22	4.8	580	9.47

oxygen atoms. More details can be found in the work of Mikulová et al. [5].

$$OSC = OSC_{Measured} - OSC_{Metal} \quad (3)$$

$$NL = \frac{OSC}{OSC_{Surf}} \quad (4)$$

Metal dispersions were calculated from H_2 chemisorption assuming a dissociative adsorption of hydrogen. The sample (0.500 g) was heated up to 350 °C, reduced for 60 min under H_2 (30 mL min^{-1}) and degassed for 180 min under Ar (30 mL min^{-1}). Hydrogen pulses were injected at −85 °C. This temperature was obtained by mixing acetone with liquid nitrogen and was necessary to avoid the participation of cerium-based supports in H_2 consumption.

Temperature-Programmed Oxidation (TPO) analyses were carried out to determine carbon contents in used catalysts. The sample (from 5 to 15 mg) was heated up to 700 °C at a ramp of 7 °C min^{-1} in a 1% O_2/He mixture (12 mL min^{-1}). The outlet gas mixture was periodically analyzed by GC in order to determine the amounts of consumed O_2 and formed CO_2. The relative error associated with this analysis is 10%.

2.4. Data analysis

The performance and the behaviour of tested catalysts were compared based on phenol conversion (Conv), Total Organic Carbon abatement (ΔTOC) and phenol mineralization (M). Details for the calculations can be found elsewhere [23].

The selectivity (S_i) in reaction product i was obtained from Eq. (5) where $F(i)$ (%) is the fraction of organic carbon converted to product i and Conv (%) is the overall conversion.

$$S_i = \frac{F(i)}{Conv} \quad (5)$$

Turnover Frequencies (TOF) were calculated according to Eq. (6) where A ($mmol_{PhOH}\,g_{Cata}^{-1}\,h^{-1}$) is the rate of disappearance of phenol, M(Me) ($g\,mol^{-1}$) is the molar mass of the supported metal, X(Me) (%) is the metal content in the catalyst and D (%) is the dispersion of the supported metal.

$$TOF(h^{-1}) = \frac{A \times M(Me) \times 10}{X(Me) \times D} \quad (6)$$

3. Results and discussion

3.1. Catalyst characterization

The physical properties of prepared supports and catalysts are listed in Table 1.

Diffraction patterns of prepared samples (not shown) only indicate the presence of a ceria fluorite-type phase. This suggests that homogeneous Ce-, Zr- and/or Pr-based oxide solid solutions are formed. Pt and Ru diffraction peaks cannot be observed, probably because metal particles are too small to be detected by XRD. At identical thermal treatment, the specific surface area (SSA) of commercial ceria is always higher than those of laboratory-prepared mixed oxides. This is attributed to the different preparation method. Support particle sizes calculated from XRD are in good agreement with those obtained from SSA in the cases of Ce- and ZrCe-based materials. On the contrary, d_{XRD} is always smaller than d_{SSA} for ZrCePr-based materials. We suggest that ZrCePr-supported catalysts have a more defective and partly amorphous structure, which leads to broader XRD peaks and therefore the underestimation of d_{XRD}. For a given oxide, an increase in the calcination temperature promotes the sintering of support particles. Similarly, for a given metal, higher reduction temperatures lead to lower dispersions. Although the SSA of Pt and Ru catalysts are comparable, the former metal is significantly better dispersed than the latter. The absolute value of ceria zeta potential is higher in alkaline medium than in acidic medium [24]. Therefore the number of ionized adsorption sites at the surface of the oxide support is higher during the preparation of Pt catalysts (alkaline pH) than during that of Ru catalysts (acidic pH), leading to better dispersions.

In the absence of a supported metal, NL values are lower than 1 for ceria and ceria–zirconia, which implies that, at the temperature of the measurement (400 °C), only oxygen atoms from the surface are available. NL values exceeding 1 are obtained upon addition of a second doping element (Pr): the presence of lattice defects activates oxygen atoms from the bulk of the oxide. In all cases, the deposition of a metal phase is beneficial to oxygen storage properties. These observations are consistent with those of Bedrane et al. [25].

3.2. Performance in CWAO

All supports and catalysts presented in Table 1 were tested in the CWAO of phenol. A blank run was also performed to assess the performance of the non-catalytic thermal process. For each experiment, it was verified that the carbon balance calculated from GC, TOC and TPO analyses after 180 min of reaction was always comprised between 90% and 110%. Some experimental curves were already presented in a previous paper [23]. The kinetic study was completed to have an in-depth knowledge about the behaviour of the catalysts in the CWAO of phenol. Yet unpublished data are shown in Fig. 1.

In the absence of a catalyst, phenol is slightly mineralized (M = 21%) after 180 min of reaction. An induction period, which is characteristic of a reaction involving a free-radical mechanism [10], can be observed at the beginning of this experiment. Phenol and TOC abatements are significantly improved in the presence of a

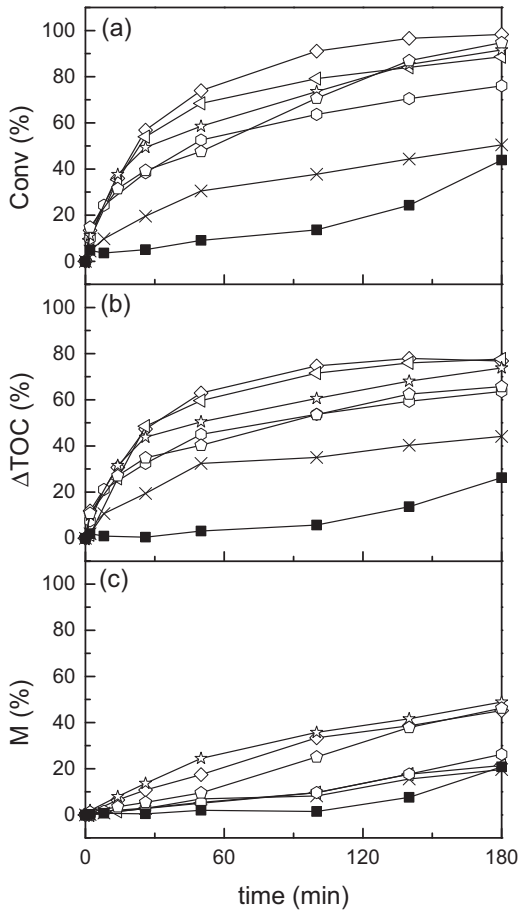

Fig. 1. (a) Phenol conversion, (b) TOC removal and (c) mineralization curves for (■) the blank experiment, (×) ZrCe650, (◊) RuZrCe500_350, (◁) RuZrCePr650_350, (⬠) RuZrCePr800_500, (☆) PtZrCe400_350 and (⚠) PtZrCePr800_800. Operating conditions: $T = 160\,^{\circ}C$, $P(O_2) = 20$ bar, $V_{Liq} = 0.16$ L, $C_{PhOH} = 2.098\ g\,L^{-1}$, $C_{Cat} = 4\ g\,L^{-1}$, $\omega = 1000$ rpm.

support or a catalyst. As a general observation, bare supports are less active than Ru catalysts, which are less efficient than Pt catalysts. Samples among each of these categories can be compared based on the mineralization rates obtained after 180 min of reaction:

$$\text{ZrCePr650} < \text{blank} \approx \text{ZrCe650} < \text{Ce650}$$

$$\text{RuZrCePr650\_350} \approx \text{RuZrCePr800\_350} \approx \text{RuZrCePr800\_500} < \text{RuCe800\_350} < \text{RuZrCe500\_350}$$

$$\text{PtZrCePr800\_350} \approx \text{PtZrCePr800\_800} < \text{PtZrCe400\_350} < \text{PtCe800\_350}$$

In all cases, higher mineralization rates are reached with Ce and ZrCe supports than with ZrCePr. This is contradictory with previous conclusions that catalysts with high redox properties are more active in the CWAO of phenol [3,14,26]. In order to illustrate the upcoming discussion, phenol conversion, TOC abatement and mineralization rates are plotted against time for a same catalyst (PtCe800_350) in Fig. 2. The significant gaps between ΔTOC and *M* values show that a non-negligible fraction of carbon is deposited on the catalytic surface. For Ce650 support and all catalysts, the ΔTOC–*M* difference increases at the beginning of the reaction,

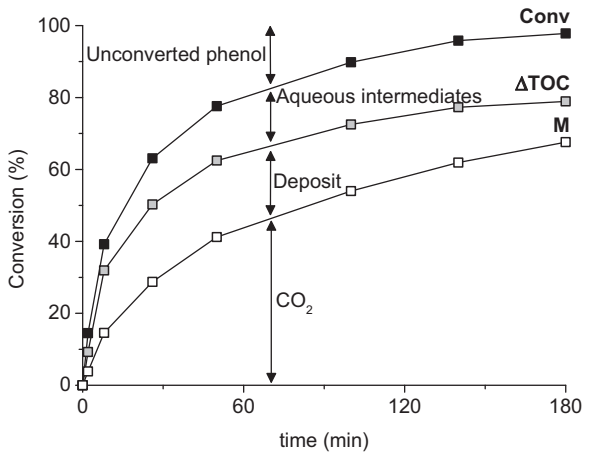

Fig. 2. Phenol conversion, TOC removal and mineralization curves for PtCe800_350.

reaches a maximum and either decreases or stabilizes. This implies that carbonaceous deposits form as soon as the reaction starts, from phenol and first intermediate species. The subsequent decrease of ΔTOC–*M* indicates the consumption of the deposit. At the end of most experiments, the rate of mineralization increases faster than the rates of phenol and TOC removal. This indicates that CO_2 does not only come from the oxidation of aqueous organic compounds but also from that of adsorbed species. Therefore the carbonaceous deposit is not a final reaction product leading to the irreversible blocking of active sites but is rather an intermediate species that temporarily limits activity. Fast adsorption followed by slower surface oxidation of C-containing species was also reported by Delgado et al. [14]. Arena et al. [26] concluded that the latter step was rate-limiting.

3.2.1. *Influence of the temperature*

To evaluate the influence of temperature on the catalytic performance, RuZrCePr800_500 was tested at 160, 180 and 200 °C. The increase in temperature significantly improves phenol and TOC conversions as well as the mineralization rate (Fig. SI1). The apparent activation energy calculated from phenol initial disappearance rate ($54\ kJ\,mol^{-1}$) is in the same range as those found in literature [15,27]. The selectivity in aqueous organic intermediates, adsorbed species and carbon dioxide determined at 50% conversion for each reaction temperature is presented in Fig. 3. The selectivity in adsorbed carbon is much lower at 200 °C owing to the easier degradation of carbonaceous deposits at higher temperature, as reported by Delgado et al. [14] and Hamoudi et al. [28]. An increase in the pH accompanied by a diminution of the Conv–ΔTOC difference is observed at the end of the experiment performed at 200 °C. This indicates the conversion of aqueous carboxylic acid intermediates. Despite this, the concentration of acetic acid continuously increases with phenol conversion, confirming the highly refractory nature of this compound [29].

3.2.2. *Influence of the metal phase*

Turnover Frequencies (TOF) were calculated at 0% and 50% conversion and plotted against metal dispersion (*D*) for Ru and Pt catalysts (Fig. 4). From data measured at the initial time of the reaction, it appears that, at equal dispersion, Pt is always more active than Ru and is therefore a better active phase for phenol CWAO. The reverse is generally observed for acetic acid oxidation [5,6]. Whatever the deposited metal, Turnover Frequencies vary with metal dispersion, which indicates that phenol oxidation is sensitive to particle size. TOF = *f*(*D*) curves obtained for Pt catalysts have the same shape as those obtained for Ru ones. This reveals a similar behaviour of the two metals. In both cases, bigger

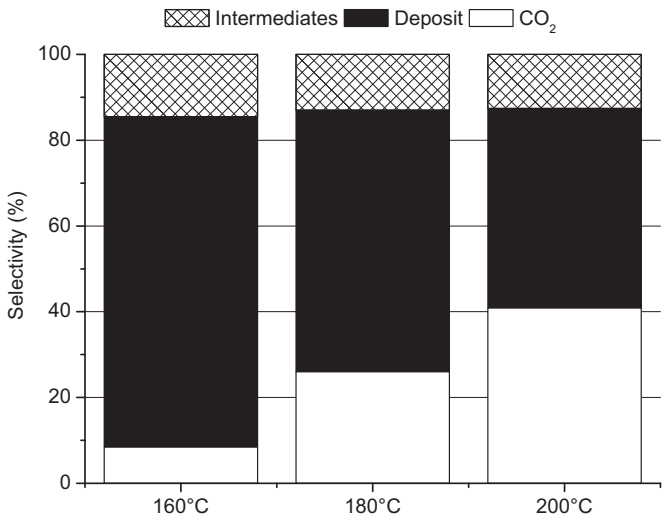

Fig. 3. Influence of temperature on the selectivity in aqueous organic intermediates, adsorbed species and carbon dioxide for RuZrCePr800_500.

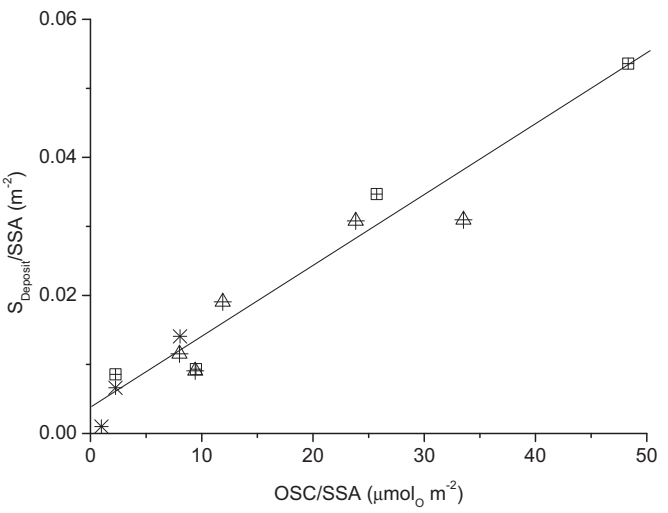

Fig. 5. Influence of the amount of available oxygen atoms on the selectivity in adsorbed carbon for (*) supports, (◇) Ru catalysts and (⊞) Pt catalysts.

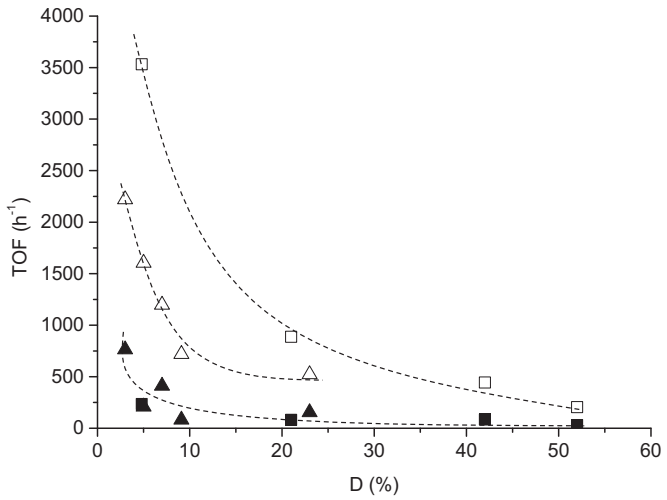

Fig. 4. Influence of metal dispersion (D) on Turnover Frequencies (TOF) for Ru (triangle symbols) and Pt catalysts (square symbols) at 0% (open symbols) and 50% conversion (filled symbols).

particles exhibit higher TOF than smaller ones. This does not necessarily mean that better specific activities (per gram) are obtained on poorly dispersed catalysts. TOF values calculated at 50% conversion are smaller than those measured at the initial time of the reaction because the concentration of phenol remaining in solution and likely to react is lower. Interestingly, experimental data points corresponding to Ru and Pt catalysts are, in that case, on a same trend curve, which probably comes from the deactivation of Pt catalysts as a result of fouling and/or overoxidation.

3.2.3. *Influence of oxygen storage properties*

The formation of carbonaceous deposits is a surface phenomenon. Considering that $S_{Deposit}$ is the selectivity in adsorbed carbon calculated at 50% conversion, the $S_{Deposit}$/SSA ratio corresponds to the amount of deposited carbon per catalyst surface unit. Similarly, because the NL values of ceria-based catalysts are inferior to 1 below 200 °C [25], oxygen storage can be considered as a surface phenomenon at the temperature of the catalytic measurements (160 °C). The surface density of available oxygen atoms is given by the OSC/SSA ratio. Fig. 5 shows the influence of OSC/SSA on $S_{Deposit}$/SSA for all supports and catalysts. We assume that the classification of catalysts based on their OSC measured at 400 °C is not modified under reaction conditions at 160 °C. This assumption is supported by the work of Bedrane et al. [25] whose data indicate that the ranking of Pt and Ru catalysts depending on their oxygen storage properties remains unchanged in the 200–500 °C temperature range and very likely at 160 °C too.

Experimental data points corresponding to bare supports are located on the same trend line as those of Ru and Pt catalysts which suggests that the distribution of reaction products (and therefore the reaction pathway) is not affected by the supported metal but is mainly governed by the nature of the support. The linear increase of $S_{Deposit}$/SSA with OSC/SSA confirms that significant OSC values favour the accumulation of adsorbed species during phenol oxidation. The corresponding straight trend line does not go through the origin of the graph. This suggests that the formation of carbonaceous deposits can also occur on samples with low OSC, as reported for certain catalysts supported on irreducible oxides such as alumina [27,30]. This observation must however be moderated owing to the very low amount of adsorbed species formed on Ce650 ($S_{Deposit}$/SSA = 0.001 m^{-2}).

ZrCePr-supported catalysts, despite their higher oxygen storage properties, produce higher amounts of adsorbed species than Ce- and ZrCe-supported catalysts, thus leading to lower performance. This conclusion seems to be in contradiction with literature as it is well known that doping ceria with Zr^{4+} and/or Pr^{4+} cations limits the accumulation of coke [31] in reactions such as methane partial oxidation [32] or dry reforming [33]. However, it is difficult to make a direct comparison because the operating conditions of the previously mentioned reactions (600–900 °C in the gas phase) greatly differ from those of CWAO, which affects both the nature and reactivity of carbonaceous deposits. Contradictory information can be found in the field of CWAO. Lee et al. [30] determined that higher amounts of carbonaceous deposits were formed on Pt/Al_2O_3 than on Pt/CeO_2 and suggested that the OSC properties of ceria could promote the oxidation of adsorbed materials. On the contrary, Kim et al. [3] observed that the amount of carbonaceous materials formed during the CWAO of phenol increased upon addition of ceria to oxides of transition metals supported on Al_2O_3. Additionally, a study concerning the CWAO of acetic acid [5] showed that materials with high NL favour the formation of deactivating hydroxycarbonates. Even though the carbonaceous deposit formed during phenol oxidation differs from such species [34], the conclusion remains that high OSC can promote the accumulation of species responsible for a decrease in activity.

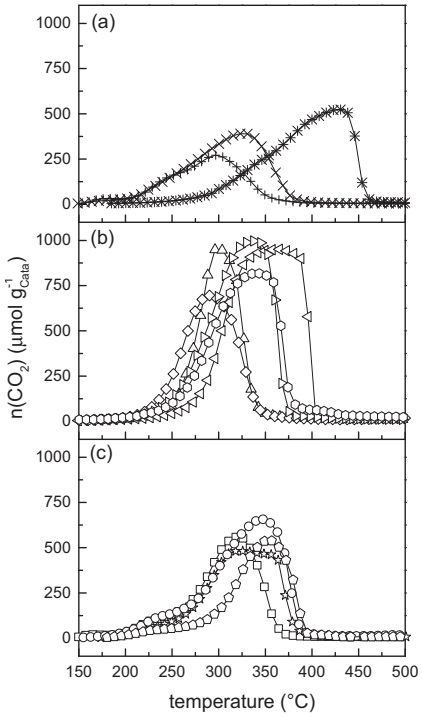

Fig. 6. TPO profiles of used (a) supports [(+) Ce650, (×) ZrCe650, (*) ZrCePr650], (b) Ru catalysts [(△) RuCe800_350, (◊) RuZrCe500_350, (◁) RuZrCePr650_350, (▷) RuZrCePr800_350, (⬠) RuZrCePr800_500] and (c) Pt catalysts [(□) PtCe800_350, (☆) PtZrCe400_350, (◯) PtZrCePr800_350, (⧋) PtZrCePr800_800].

CO_2 formation profiles recorded during the TPO of used supports and catalysts are presented in Fig. 6. It was verified by mass spectrometry that only H_2O and CO_2 form under TPO conditions. The combustion of adsorbed species takes place between 200 and 500 °C, in agreement with literature data [3,27,35]. Most of CO_2 production profiles do not exhibit a symmetric Gaussian shape. This indicates that the combustion of adsorbed species occurs in several steps giving rise to successive overlapping oxidation peaks. It is known that molecules adsorbed in the proximity of noble metal particles can be oxidized at lower temperature [27,30]. However, in the present study, several oxidation peaks are visible even in the case of bare supports and no additional combustion peaks appear in the presence of a metal phase. This suggests that several types of carbonaceous deposits, which burn off at different temperatures, coexist on the catalytic surface (for example, both low-weight aliphatic adsorbates and heavy aromatic polymers were shown to form during phenol oxidation [3,10,28]).

Hereunder, supports, Ru catalysts and Pt catalysts are respectively sorted by increasing temperature of starting combustion of carbonaceous deposits during TPO.

$$\text{Ce650} \approx \text{ZrCe650} < \text{ZrCePr650}$$

$$\text{RuZrCe500\_350} < \text{RuCe800\_350} < \text{RuZrCePr800\_350} < \text{RuZrCePr800\_500} < \text{RuZrCePr650\_350}$$

$$\text{PtCe800\_350} \approx \text{PtZrCePr800\_350} < \text{PtZrCe400\_350} < \text{PtZrCePr800\_800}$$

Samples for which the combustion of adsorbed species starts at lower temperature can be considered as more active in the oxidation of carbon deposits. With the exception of PtZrCePr800_350,

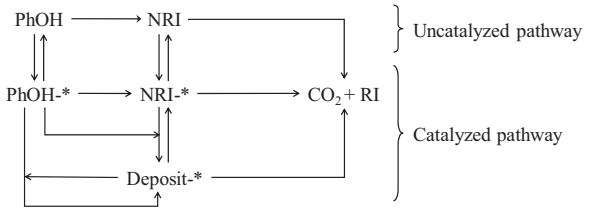

Fig. 7. Detailed reaction scheme for phenol oxidation.

TPO results are consistent with the previous rankings based on phenol CWAO performance. This confirms that materials with low OSC can more easily degrade adsorbed species and are hence more efficient in CWAO. One could argue that the reason for this could be that active oxygen species in ZrCePr, although more numerous, may be less reactive than those in Ce and ZrCe. Nevertheless, temperature-programmed reduction experiments show that this is not the case (Fig. SI2). Since carbonaceous deposits come from a partial oxidation reaction [34] involving the very first intermediates of phenol oxidation, we suggest that their formation is accompanied with a depletion of surface reactive oxygen species. A high coverage of the catalytic surface by these adsorbed species could hinder the reoxidation of the material, thus limiting its oxidation capability. This phenomenon could be worsened in the case of ZrCePr because the incorporation of Pr to ceria increases the basicity of the material [36,37], which was reported to favour polymerization reactions [38]. A second explanation could be that high OSC properties enhance the overoxidation of noble metal particles, which was also reported to favour the formation of polymeric products [13]. It was not possible to experimentally rule out any of these hypotheses. In particular, the combustion of fouling materials under OSC measurement conditions did not allow us to determine the OSC of used catalysts.

3.3. Kinetic modelling

3.3.1. Reaction pathway

Based on the conclusions reached in the previous paragraphs, phenol oxidation can be represented by the reaction scheme given in Fig. 7. Since many intermediate species form in the course of the reaction, carbon-containing compounds are lumped into categories depending on their reactivity. Phenol (PhOH) is oxidized following two reaction pathways: a non-catalytic homogeneous pathway, which was demonstrated by the non-null activity of the blank experiment, and a heterogeneously catalyzed pathway, which was confirmed by the increase in activity provided by a catalytic system. Phenol is first degraded into Non-Refractory Intermediates (NRI) such as hydroquinone, benzoquinones and catechol. These easily oxidizable organic species can be converted to final products of the reaction, namely CO_2 and Refractory Intermediates (RI), such as acetic acid. Phenol and reaction intermediates can reversibly adsorb on catalytic sites (*). Adsorbed compounds can either be degraded into smaller molecules or take part in condensation reactions, leading to the formation of heavier organic species (Deposit). The polymerization reaction does not necessarily stop at this stage as the growing polymer can react again with phenol or organic intermediates to form trimers, tetramers, etc. The so-formed high-molecular-weight adsorbate can be degraded into smaller compounds and final products of the reaction.

In order to increase the ease of use of the proposed reaction scheme, the latter was simplified to a triangular model inspired by that proposed by Li et al. [39] in 1991. The non-catalytic reaction pathway was neglected and only three categories of compounds were kept including (i) Non-Refractory Compounds (NRC = PhOH + NRI), (ii) adsorbed species without discrimination

Table 2
Optimized parameters obtained by kinetic modelling.

Catalyst	k_1 (L mol^{-1} min^{-1})	k_2 (L mol^{-1} min^{-1})	$k_3 \times 10^2$ (min^{-1})	$\bar{C_T}$ (mol$_C$ L^{-1})
Ce650	0.00	0.67	1.60	0.023
ZrCe650	0.04	0.36	0.43	0.040
ZrCePr650	0.02	0.18	0.23	0.044
RuCe800_350	0.09	0.21	0.41	0.067
RuZrCe500_350	0.21	0.77	0.53	0.066
RuZrCePr650_350	0.05	0.50	0.21	0.091
RuZrCePr800_350	0.03	0.29	0.52	0.059
RuZrCePr800_500	0.00	0.51	0.42	0.062
PtCe800_350	1.41	0.80	0.49	0.031
PtZrCe400_350	0.63	1.48	0.77	0.040
PtZrCePr800_350	0.11	1.16	0.58	0.056
PtZrCePr800_800	0.15	1.11	1.31	0.049

between light and heavy carbonaceous materials (Deposit) and (iii) the Final Products of the reaction (FP = CO_2 + RI). The corresponding chemical and kinetic equations are presented in Fig. 8. Neglecting the non-catalytic reaction pathway is a simplification that deserves discussion. It is true that the mineralization rate of 21% obtained during the blank experiment is not a value that should, a priori, be considered negligible, in particular compared to those obtained in the presence of ZrCe650 (20%), ZrCePr650 (8%), RuZrCePr650_350 (21%) or RuZrCePr800_350 (25%). However, it is important to take into account that the reaction pathway is modified in the presence of a catalyst: the fast formation of carbonaceous deposits results in a significant decrease in the concentration of aqueous phenol, which greatly lowers the rate of the non-catalytic phenol mineralization. Oxygen pressure being maintained constant throughout the reaction, it is assumed that oxygen concentration does not vary and that kinetic and adsorption terms corresponding to this reactant can be incorporated into k_1, k_2 and k_3 rate constants. All active sites are supposed to be similar and reaction orders with respect to each category of compounds are assumed to be 1. The suggested model does not take into account that irreversible changes in the catalytic structure, such as leaching, sintering or overoxidation, can occur during the reaction, leading to gradual deactivation.

In the above formulas, $C_{Deposit}$ and $\bar{C_V}$ are the respective concentrations of adsorbed carbon and vacant adsorption sites at the surface of the catalyst. They are expressed in mol$_C$ m$^{-2}_{Cata}$ and can eventually be converted to mol$_C$ g$^{-1}_{Cata}$ or mol$_C$ L$^{-1}_{Solution}$. Their sum is $\bar{C_T}$ (Eq. (7)), which is the maximal amount of carbon that can be deposited over the catalyst surface [15,23,35,38].

$$\bar{C_T} = C_{Deposit} + \bar{C_V} \quad (7)$$

3.3.2. Optimized parameters

k_1, k_2, k_3 and $\bar{C_T}$ were determined from experimental concentrations expressed in mol$_C$ L^{-1} (Table 2) by a nonlinear least squares minimization method. A good agreement was obtained between experimental and modelled data (R^2 was always in the range of 0.978–0.998), as illustrated in Fig. 9 for RuCe800_350 catalyst.

Globally, k_1, k_2 and k_3 rate constants increase with metal dispersion (Fig. 10a–c), which confirms the key-role of this parameter. A higher dispersion implies (i) a larger amount of surface metal atoms capable of oxidizing aqueous compounds as well as (ii) a better distribution of active metal species on the catalyst surface, which promotes the elimination of adsorbed species and therefore limits their accumulation [40].

Below, supports, Ru catalysts and Pt catalysts are sorted by increasing value of k_3, which is the rate constant associated with the degradation of adsorbed compounds.

ZrCePr650 < ZrCe650 < Ce650

RuZrCePr650_350 < RuZrCePr800_500 ≈ RuCe800_350 < RuZrCePr800_350 < RuZrCe500_350

PtCe800_350 < PtZrCePr800_350 < PtZrCe400_350 < PtZrCePr800_800

This classification is virtually identical to those obtained from mineralization rates and TPO analyses. This confirms that k_3 rate constant is representative of the catalyst ability to degrade carbonaceous deposits under CWAO and TPO conditions. Some exceptions have to be noted: k_3 seems overestimated in the case of PtZrCePr800_800 and underestimated in the cases of RuCe800_350 and PtCe800_350. One may also notice that k_1 is null for Ce650 and RuZrCePr800_500, which is compensated by high values of k_2 and k_3. Those incoherencies probably result from the hypotheses associated with our model and the limited amount of experimental data employed during optimization.

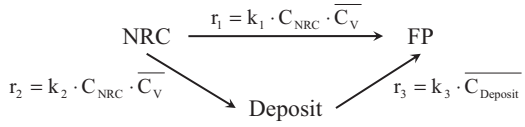

Fig. 8. Simplified reaction scheme for phenol oxidation.

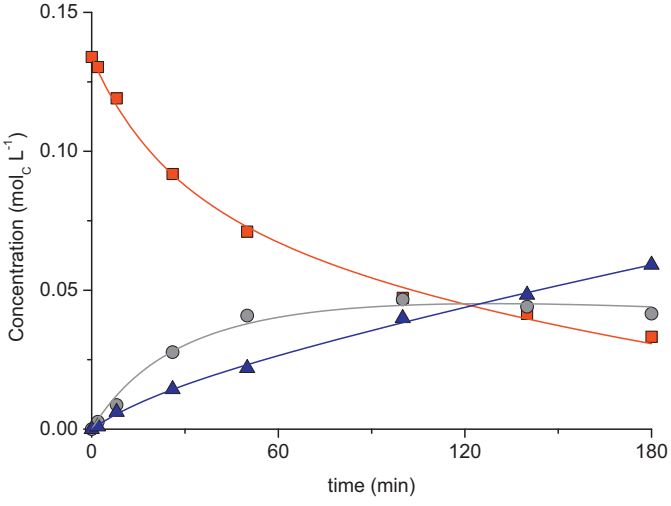

Fig. 9. Experimental (symbols) and modelled (lines) concentrations of NRC (⬠), Deposit (■) and FP (●) for RuCe800_350.

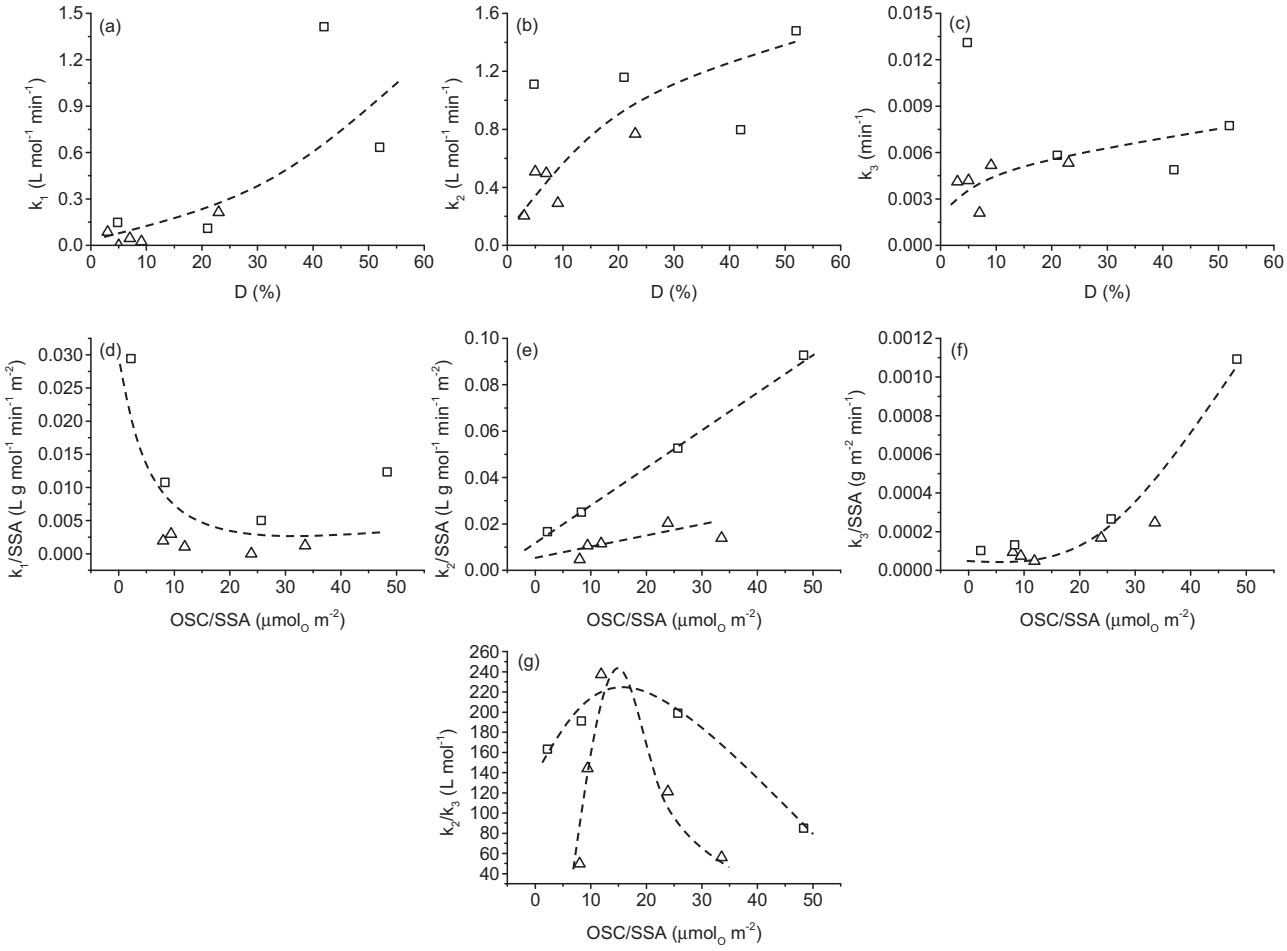

Fig. 10. Influence of noble metal dispersion and OSC on reaction rate constants for (△) Ru and (□) Pt catalysts.

As previously mentioned, fouling and OSC are surface phenomena. On the other hand, reaction rate constants were determined for a given mass of catalyst and must therefore be normalized to the specific surface area of the material in order to be representative of the reaction kinetics occurring at the surface of the catalyst. In agreement with previous conclusions, increased OSC/SSA values result in increased k_2/SSA (Fig. 10e) and decreased k_1/SSA (Fig. 10d), confirming that high OSC favour the formation of carbonaceous deposits while the direct surface oxidation of phenol is hindered as a result of overoxidation and/or fouling. Besides that, k_3/SSA increases with increasing OSC/SSA (Fig. 10f) suggesting that OSC properties enhance the oxidation of carbonaceous deposits. This seems to be in contradiction with previous observations that high OSC catalysts produce less CO_2 in phenol CWAO and burn carbonaceous deposits at higher temperatures in TPO. However, these discrepancies can easily be explained by considering that catalytic tests are performed on initially fresh samples and that, after 180 min of reaction, samples with high OSC (and therefore high k_2/SSA) are more deactivated (either by overoxidation or fouling) than those with low OSC. Therefore, the proposed model allows to extract information which are otherwise not directly available at the end of a short-term experiment, since samples are not deactivated to the same extent. Another point worth mentioning is that the k_2/k_3 ratio first increases with increasing OSC/SSA then goes through a maximum and decreases (Fig. 10g). This indicates that deactivation by fouling can be limited by using catalysts with either low or high OSC properties, on which carbonaceous deposits are either not likely to form or readily degraded, respectively.

The maximal carbon contents in fouled catalysts ($\%C_{Max}$) calculated from the optimized values of $\bar{C}_T$ range from 6.4 to 21.4 wt%. These values are in the same range as those experimentally determined by Hamoudi et al. ($\%C_{Max}$ = 22 wt%) [15] and Delgado et al. ($\%C_{Max}$ = 20 wt%) [35].

4. Conclusions

Three oxide supports were synthesized, from which nine monometallic Pt- or Ru-based catalysts were prepared, characterized and tested in the Catalytic Wet Air Oxidation (CWAO) of phenol. These catalysts were evaluated in terms of phenol mineralization and resistance to fouling. A simplified reaction scheme was successfully used to describe the reaction. Experimental observations and modelled parameters were generally in good agreement but some discrepancies could be noted, indicating that additional experimental data were needed to achieve better optimization of rate constants.

Three key-parameters were found to control the performance in the CWAO of phenol:

(1) The nature of the metal phase plays an important role in activity. In the fresh state, Pt-based catalysts are, at similar dispersion, more active than Ru ones. However, the difference in activity of the two noble metals seems to be reduced on aged samples.
(2) High metal dispersions lead to improved performance. A better coverage of the oxide surface by metal particles promotes the oxidation of aqueous organic species and the degradation of adsorbed compounds.

(3) The Oxygen Storage Capacity (OSC) of ceria is greatly improved by doping with Zr^{4+} and Pr^{4+} cations as well as the presence of supported noble metal particles. Contrary to what was expected, very high OSC are detrimental to the activity and stability of fresh catalysts. The increase in the number of surface oxidation sites favours the formation of adsorbed heavy species which accumulate on the surface and are thought to block the redox cycle by limiting the reoxidation of the catalytic site. Overoxidation of noble metal particles could also be partly responsible for activity decrease. On the other hand, results of the kinetic modelling indicate that high OSC also enhance the degradation of fouling species. Therefore, deactivation by fouling can be limited by using catalysts with either low or high OSC properties, on which carbonaceous deposits are either not likely to form or readily degraded, respectively.

Appendix A. Supplementary data

Supplementary data associated with this article can be found, in the online version, at http://dx.doi.org/10.1016/j.apcatb.2013.12.028.

References

[1] V.S. Mishra, V.V. Mahajani, J.B. Joshi, Ind. Eng. Chem. Res. 34 (1995) 2–48.
[2] S.S. Lin, C.L. Chen, D.J. Chang, C.C. Chen, Water Res. 36 (2002) 3009–3014.
[3] S.K. Kim, S.K. Ihm, Top. Catal. 33 (2005) 171–179.
[4] S. Imamura, M. Nakamura, N. Kawabata, J. Yoshida, S. Ishida, Ind. Eng. Chem. Prod. Res. Dev. 25 (1986) 34–37.
[5] J. Mikulová, S. Rossignol, J. Barbier Jr., D. Mesnard, C. Kappenstein, D. Duprez, Appl. Catal. B: Environ. 72 (2007) 1–10.
[6] D. Duprez, F. Delanoë, J. Barbier Jr., P. Isnard, G. Blanchard, Catal. Today 29 (1996) 317–322.
[7] H. Ohta, S. Goto, H. Teshima, Ind. Eng. Chem. Fundam. 19 (1980) 180–185.
[8] A. Santos, P. Yustos, A. Quintanilla, S. Rodríguez, F. García-Ochoa, Appl. Catal. B: Environ. 39 (2002) 97–113.
[9] F.J. Rivas, S.T. Kolaczkowski, F.J. Beltrán, D.B. McLurgh, Chem. Eng. Sci. 53 (1998) 2575–2586.
[10] A. Pintar, J. Levec, J. Catal. 135 (1992) 345–357.
[11] A. Eftaxias, J. Font, A. Fortuny, A. Fabregat, F. Stüber, Appl. Catal. B: Environ. 67 (2006) 12–23.
[12] A. Alejandre, F. Medina, A. Fortuny, P. Salagre, J.E. Sueiras, Appl. Catal. B: Environ. 16 (1998) 53–67.
[13] Z.P.G. Masende, B.F.M. Kuster, K.J. Ptasinski, F.J.J.G. Janssen, J.H.Y. Katima, J.C. Schouten, Catal. Today 79–80 (2003) 357–370.
[14] J.J. Delgado, X. Chen, J.A. Pérez-Omil, J.M. Rodríguez-Izquierdo, M.A. Cauqui, Catal. Today 180 (2012) 25–33.
[15] S. Hamoudi, K. Belkacemi, F. Larachi, Chem. Eng. Sci. 54 (1999) 3569–3576.
[16] F. Arena, C. Italiano, A. Raneri, C. Saja, Appl. Catal. B: Environ. 99 (2010) 321–328.
[17] F. Arena, C. Italiano, L. Spadaro, Appl. Catal. B: Environ. 115–116 (2012) 336–345.
[18] S. Rossignol, C. Descorme, C. Kappenstein, D. Duprez, J. Mater. Chem. 11 (2001) 2587–2592.
[19] K.H. Kim, S.K. Ihm, J. Hazard. Mater. 186 (2011) 16–34.
[20] S. Keav, J. Barbier Jr., D. Duprez, Catal. Sci. Technol. 1 (2011) 342–353.
[21] C. Perego, S. Peratello, Catal. Today 52 (1999) 133–145.
[22] B. Renard, Ph.D. Thesis of the University of Poitiers, 2004.
[23] S. Keav, A. Martin, J. Barbier Jr., D. Duprez, Catal. Today 151 (2010) 143–147.
[24] Z. Zhang, L. Yu, W. Liu, Z. Song, Appl. Surf. Sci. 256 (2010) 3856–3861.
[25] S. Bedrane, C. Descorme, D. Duprez, Catal. Today 75 (2002) 401–405.
[26] F. Arena, G. Trunfio, J. Negro, L. Spadaro, Appl. Catal. B: Environ. 85 (2008) 40–47.
[27] S. Hamoudi, F. Larachi, A. Sayari, J. Catal. 177 (1998) 247–258.
[28] S. Hamoudi, F. Larachi, A. Adnot, A. Sayari, J. Catal. 185 (1999) 333–344.
[29] W.J. Fisher, Water Res. 5 (1971) 187–201.
[30] D.K. Lee, D.S. Kim, Y.K. Lee, S.E. Jeong, N.T. Le, M.J. Cho, S.D. Henam, Catal. Today 154 (2010) 244–249.
[31] E.E. Iojoiu, M.E. Domine, T. Davidian, N. Guihaume, C. Mirodatos, Appl. Catal. A: Gen. 323 (2007) 147–161.
[32] S. Fangli, S. Meiqing, F. Yanan, W. Jun, W. Duan, J. Rare Earths 25 (2007) 316–320.
[33] V. Sadykov, V. Muzykantov, A. Bobin, N. Mezentseva, G. Alikina, N. Sazonova, E. Sadovskaya, L. Gubanova, A. Lukashevich, C. Mirodatos, Catal. Today 157 (2010) 55–60.
[34] S. Keav, A. Martin, J. Barbier Jr., D. Duprez, C. R. Chimie 13 (2010) 508–514.
[35] J.J. Delgado, J.A. Pérez-Omil, J.M. Rodríguez-Izquierdo, M.A. Cauqui, Catal. Commun. 7 (2006) 639–643.
[36] M. Kosmulski, Surface Charging and Points of Zero Charge, CRC Press, Boca Raton, 2009.
[37] N. Li, C. Descorme, M. Besson, Appl. Catal. B: Environ. 76 (2007) 92–100.
[38] M. Abecassis-Wolfovich, M.V. Landau, A. Brenner, M. Herskowitz, Ind. Eng. Chem. Res. 43 (2004) 5089–5097.
[39] L. Li, P. Chen, E.F. Gloyna, AIChE J. 37 (1991) 1687–1697.
[40] S. Nousir, S. Keav, J. Barbier Jr., M. Bensitel, R. Brahmi, D. Duprez, Appl. Catal. B: Environ. 84 (2008) 723–731.